Electronic Supplementary Material (ESI) for Materials Advances.

Supporting information

$PtSe_2$ on a reduced graphene foil for the alkaline hydrogen evolution reaction

Filipa M. Oliveira,[a] Iryna Danylo,[b] Vlastimil Mazánek,[a] Martin Veselý,[b] Rui Gusmão,[a] Zdeněk Sofer[a]**

[a] Department of Inorganic Chemistry, Faculty of Chemical Technology, University of Chemistry and Technology Prague, Technická 5, 166 28 Prague 6, Czech Republic
[b] Department of Organic Technology, Faculty of Chemical Technology, University of Chemistry and Technology Prague, Technická 5, 166 28 Prague 6, Czech Republic
* Corresponding authors. E-mail addresses: rui.gusmao@vscht.cz (Rui Gusmão); zdenek.sofer@vscht.cz (Zdeněk Sofer)

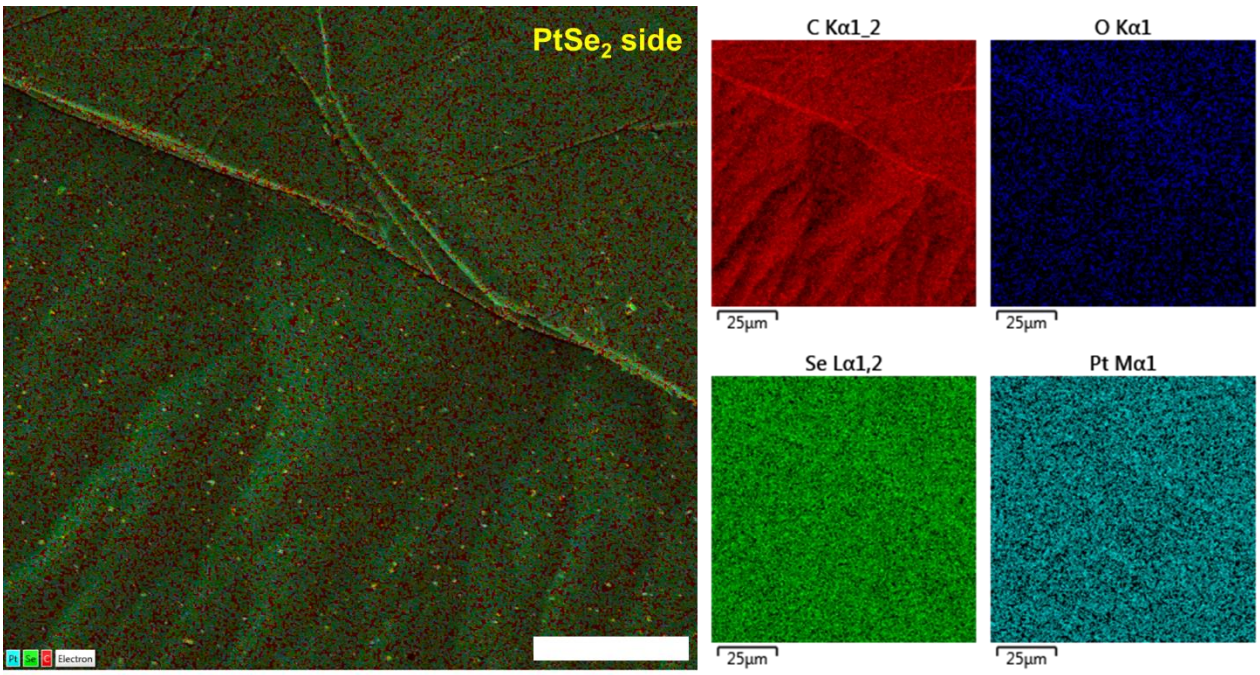

Fig. S1 EDS mapping of elements in $PtSe_2$/rGO foil on the $PtSe_2$ side. Scale bars represent 25 μm.

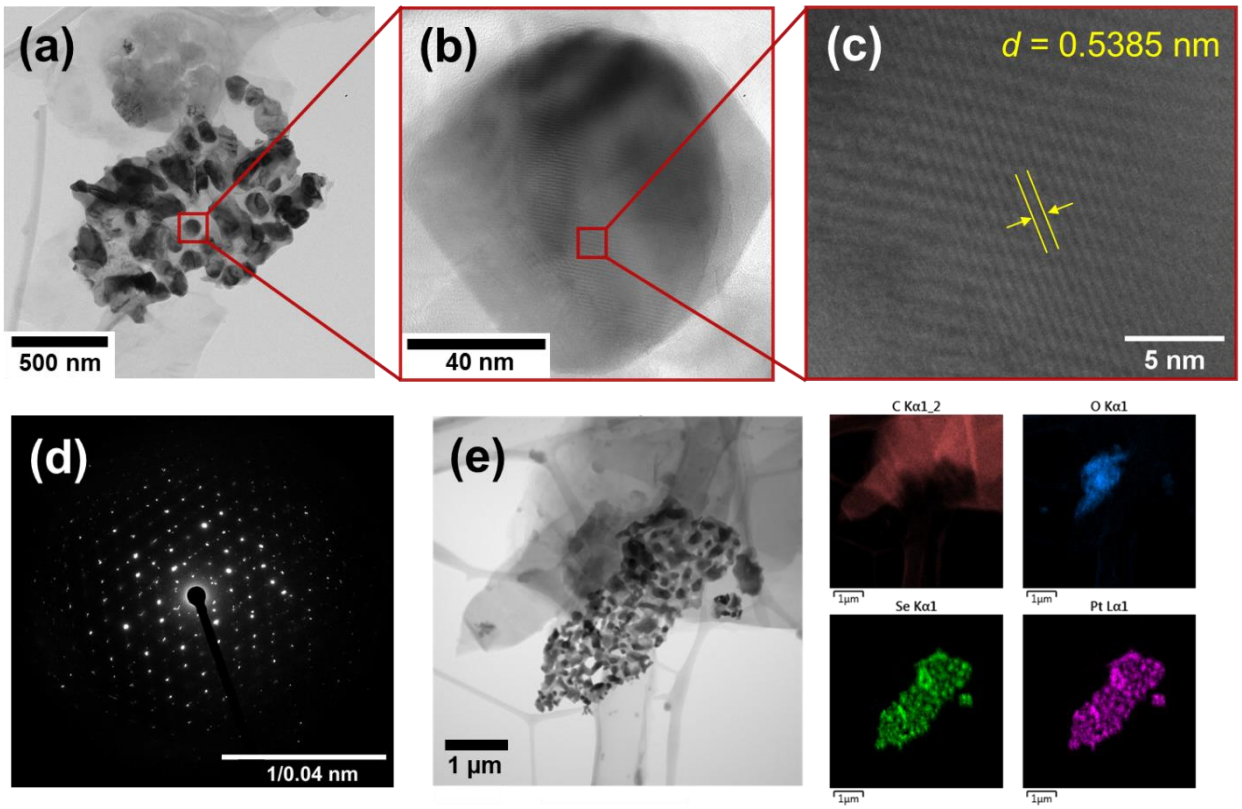

Fig. S2 (a) TEM image of $PtSe_2$ on the $PtSe_2$ side with (b) a detail of the $PtSe_2$ surface profile by HR-TEM and (c) *d*-spacing measurement. (d) Corresponding SAED pattern. (e) Mapping of respective elements C, O, Se and Pt. Scale bars in the mapping of elements represent 1 µm.

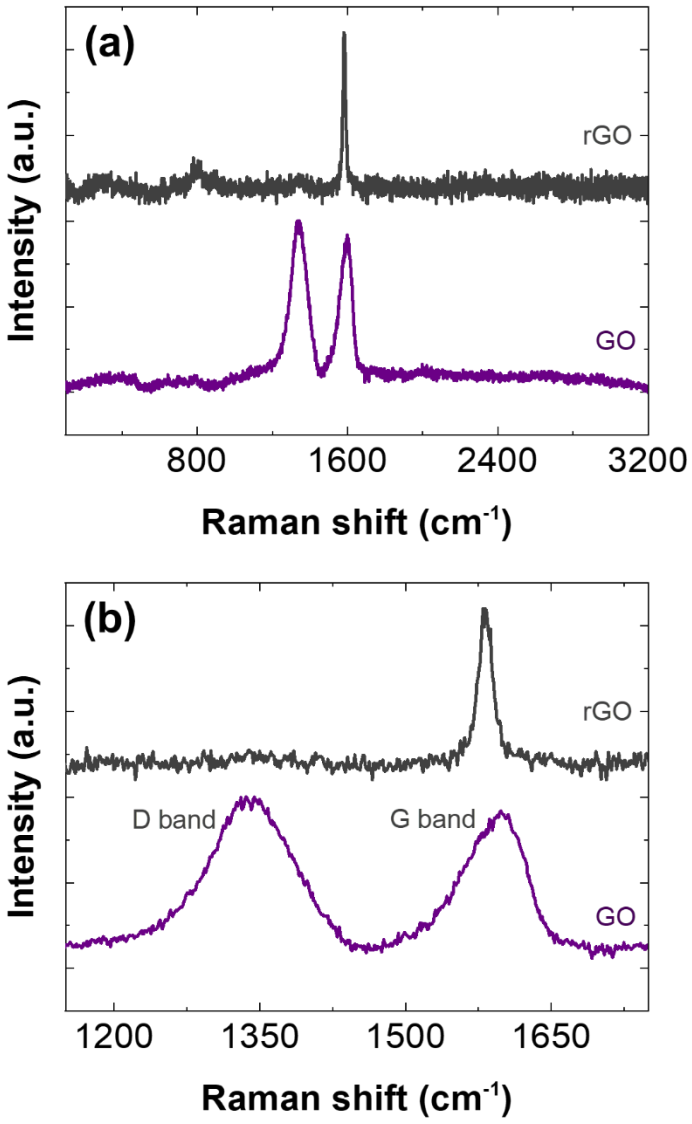

Fig. S3 Comparison of the Raman spectra of GO and rGO foil.

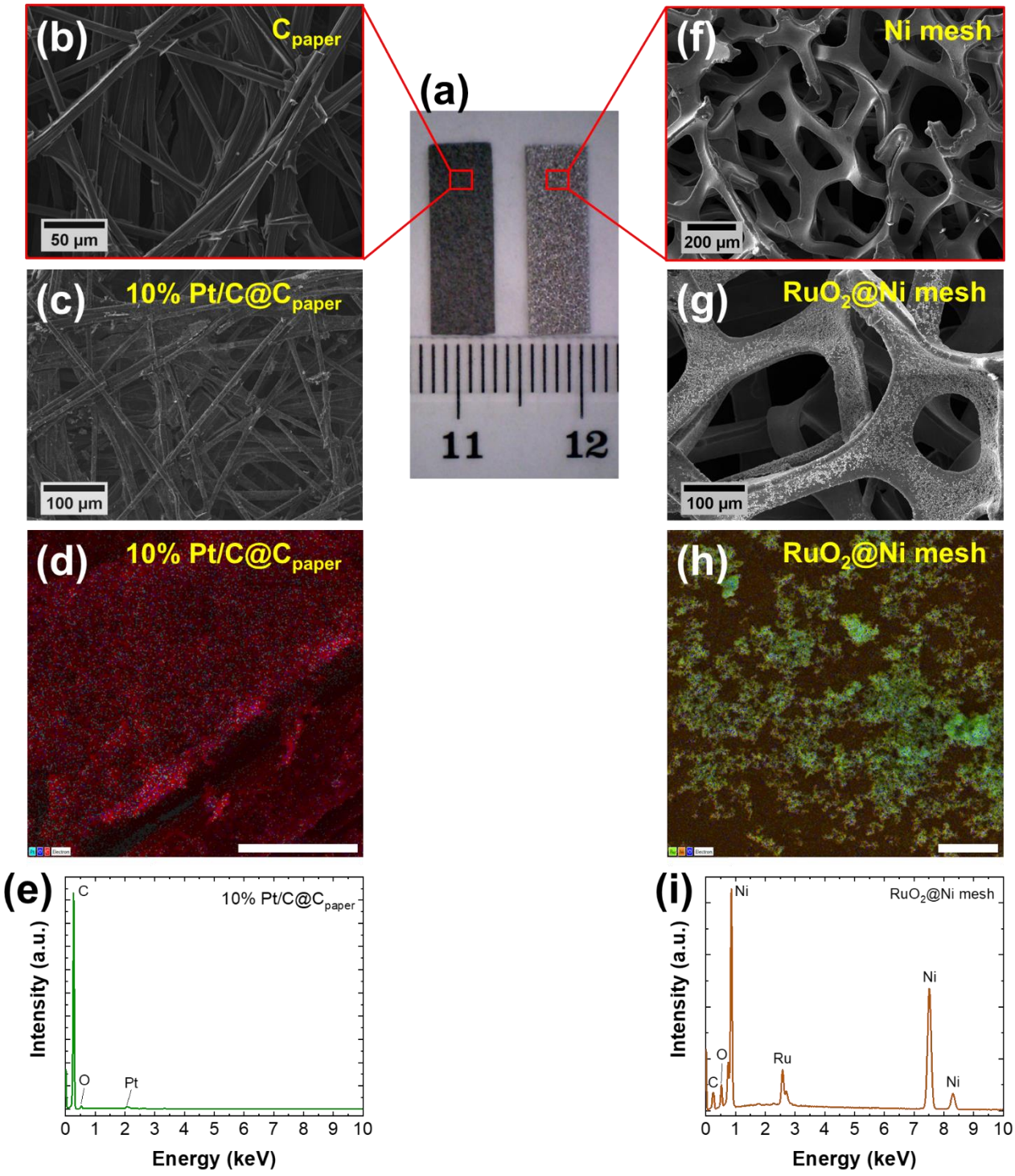

Fig. S4 (a) Photograph of unmodified C_{paper} (left) and Ni mesh (right). SEM micrograph of (b) unmodified C_{paper} and (c) 10% Pt/C@C_{paper}. (d) Mapping of the elements in 10% Pt/C@C_{paper} and (e) respective EDS spectrum. SEM micrograph of (f) unmodified Ni mesh and (g) RuO_2@Ni mesh. (h) Mapping of the elements in RuO_2@Ni mesh and (i) respective EDS spectrum. In micrographs (d) and (h), scale bars represent 25 µm.

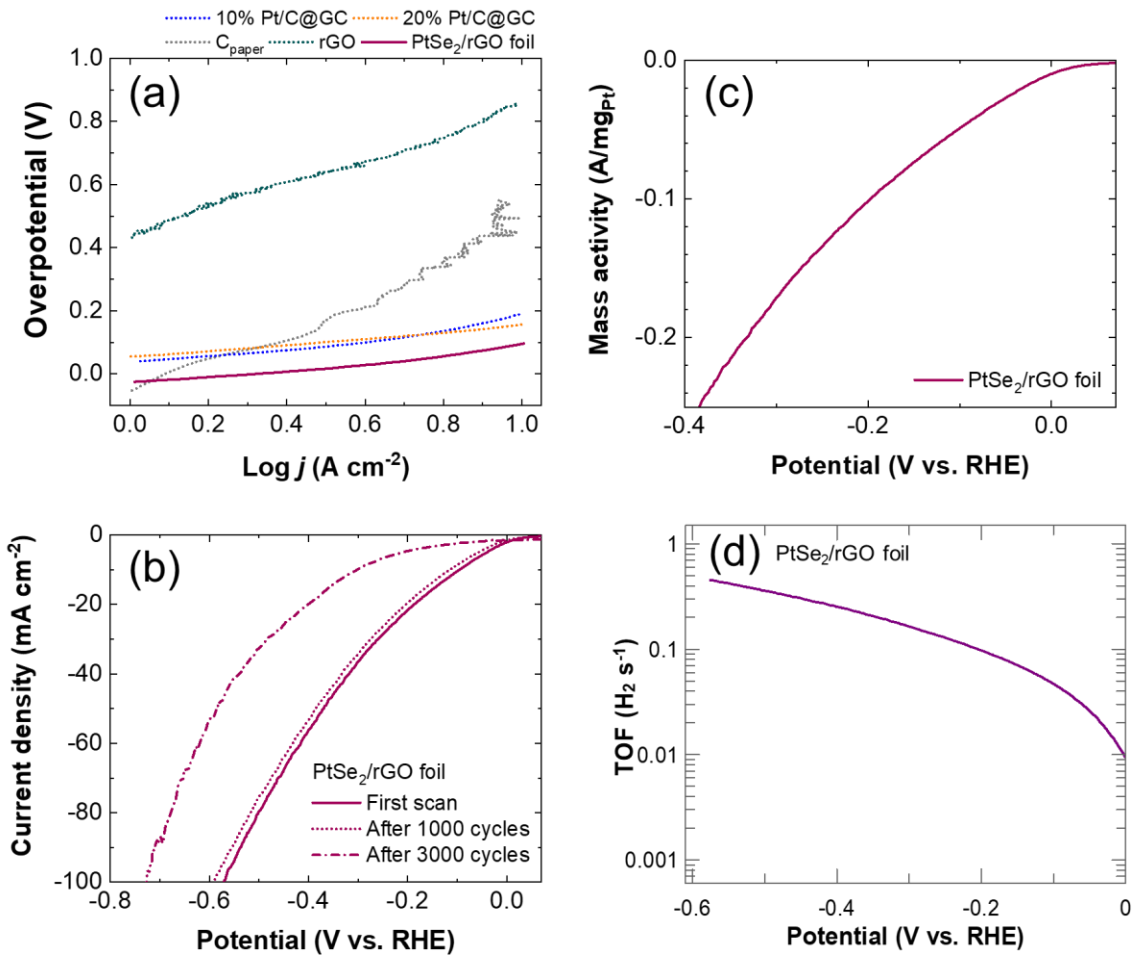

Fig. S5 HER performance in 1.0 M KOH: (a) Tafel slope curves extracted from LSV curves in Fig. 3b. (b) LSV polarization curves of $PtSe_2$/rGO foil after 3000 cycles (short dash dot) in comparison with polarization curves before (solid line) and after 1000 cycles (short dot) at 2 mV s^{-1}. c) Mass activity of $PtSe_2$/rGO. d) TOF of $PtSe_2$/rGO.

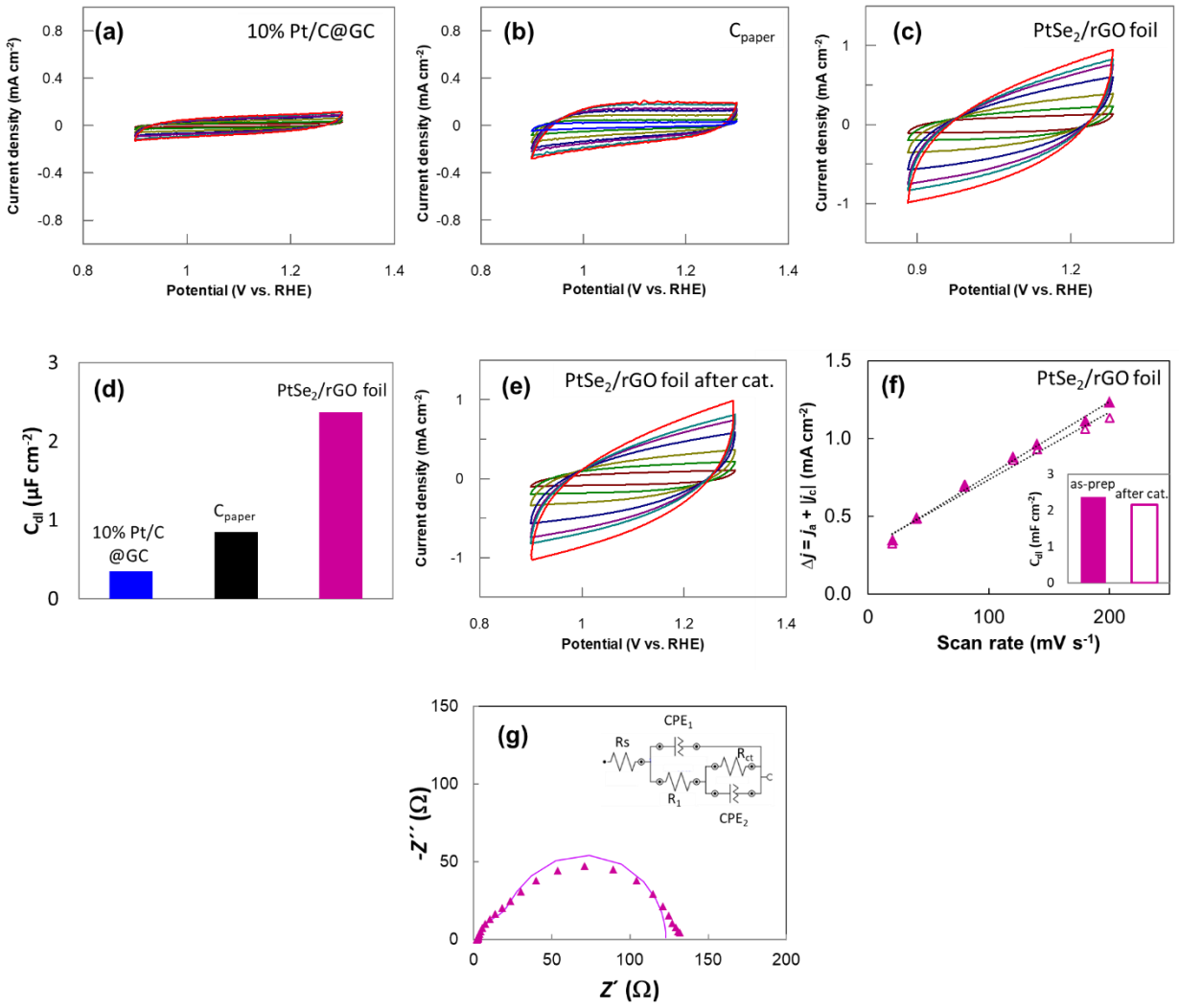

Fig. S6 Cyclic voltammograms of (a) 10% Pt/C@GC (b) C_{paper}, and (c) $PtSe_2$/rGO foil, at different rates ranging from 20−200 mV s^{-1} in the potential region from 0.9−1.3 V *vs*. RHE. (d) Column graphs with the C_{dl} values of each electrode. Cyclic voltammograms of (e) used $PtSe_2$/rGO foil using same conditions. (f) Plots of the capacitive current density at 1.1 V *vs.* scan rate, the corresponding slope can be used for determining C_{dl}. (g) Detailed of the Nyquist plot for $PtSe_2$/rGO foil at -80 mV vs. RHE, with the inset of the electrocnic equivalent circuit.

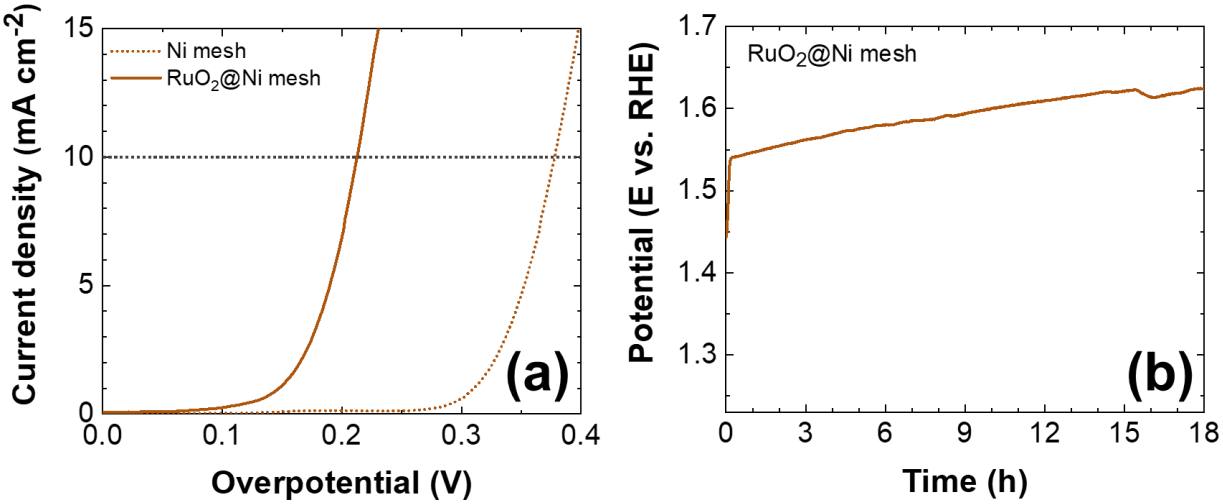

Fig. S7 (a) LSV polarization curves of Ni mesh and RuO_2@Ni mesh in 1 M KOH at 2 mV s^{-1} toward OER. (b) Long-term stability HER test of RuO_2@Ni mesh by chronopotentiometry at a fixed current density of -10 mA cm^{-2} for 18 h in 1.0 M KOH in a three-electrode configuration.

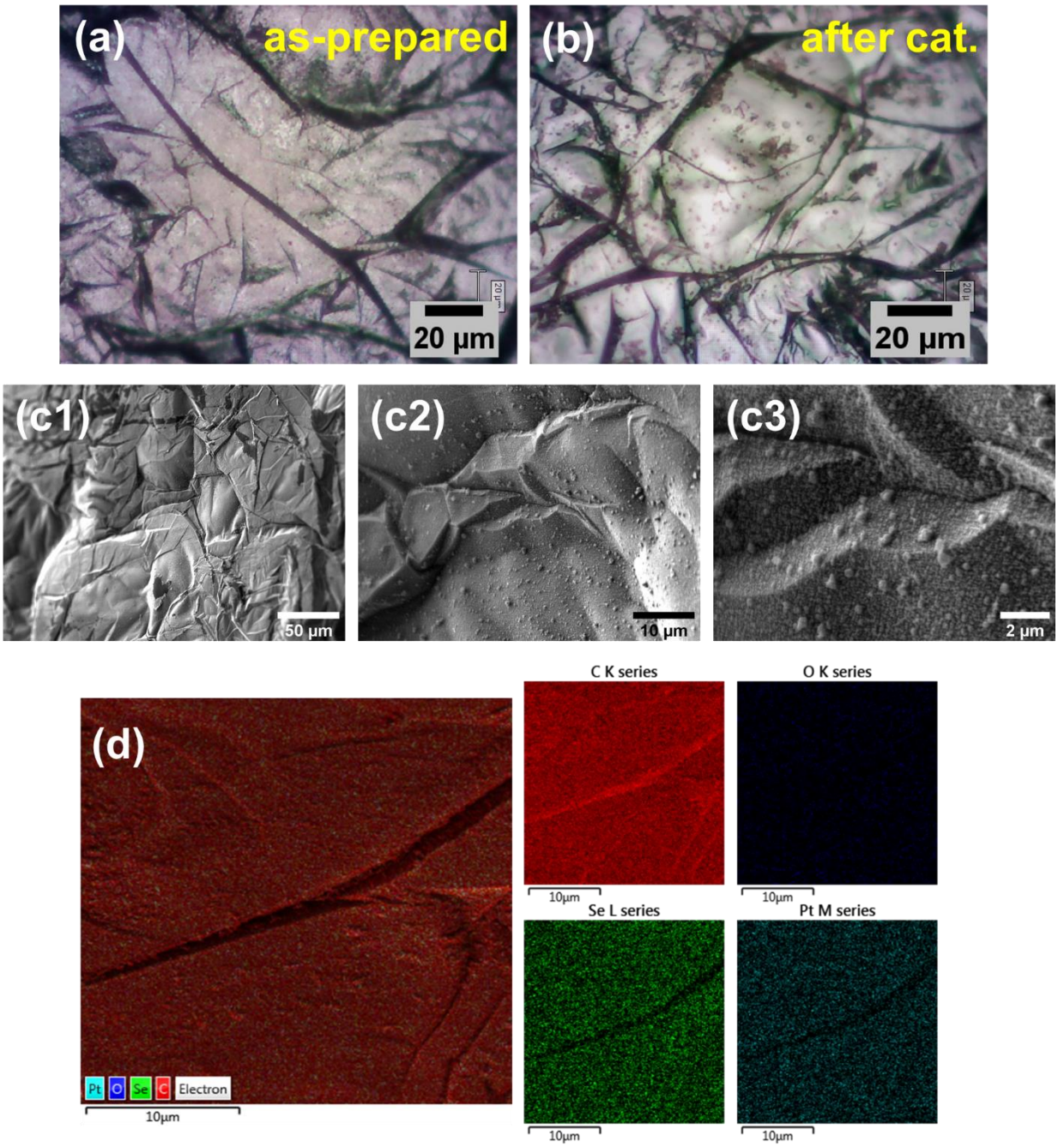

Fig. S8 Characterization of $PtSe_2$/rGO foil on the $PtSe_2$ side. Optical images of (a) as-prepared and (b) after long-term stability tests. (c1-c3) SEM micrographs at different magnifications after long-term stability tests. (d) EDS mapping of elements after long-term stability tests.

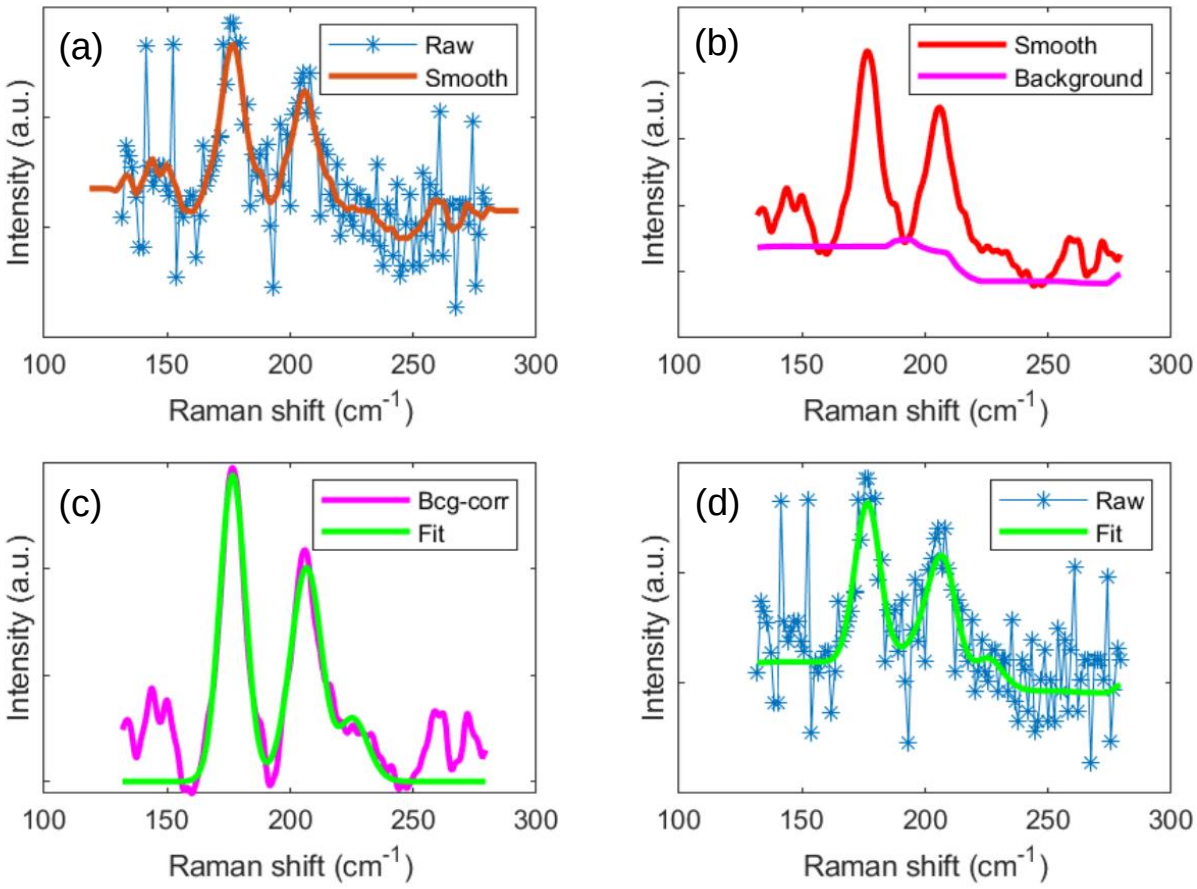

Fig. S9 Processing workflow of individual Raman spectrum in the Raman mapping. (a) Smoothen of the raw data with moving mean with local three-point values. (b) Background detection determined from the smoothen signal. (c) Automatic recognition of number of peak in background-corrected spectrum within Raman shift between 150 and 250 cm^{-1}, in which the A_{1g} and E_g vibrational modes exist. The number of identified peak was used as a number of Gaussian peaks used for fitting of the background-corrected spectrum. (d) Quality control of the Gaussian fit on the original raw signal within the Raman shift range specified in (c). Then, Gaussian parameters describing A_{1g} and E_g vibrational states are used to determine exact peak position and intensity of the fit on the raw data.

Table S1 EDS quantification of elements (at. %) in $PtSe_2$/rGO foil.

Element	$PtSe_2$ side	rGO side
C	92.7	97.4
Se	4.1	0
Pt	2.2	0
O	1.0	2.6
Total	100	100

Table S2 Comparison of the electrocatalytic activity of $PtSe_2$/rGO foil with other metal diselenide and platinum materials for HER in alkaline media.

Material	Substrate	Scan rate [mV s^{-1}]	η_{10} [mV] [a]	Tafel slope [mV dec^{-1}]	Ref.
$PtSe_2$/rGO foil	-	2	95	120	This work
rGO	-		857	391	
C_{paper}	-		552	506	
10% Pt/C	GC		191	152	
20% Pt/C			157	100	
$Sn_{11.2\%}$-$CoSe_2$	CC [b]	2	117	86	[1]
Co_9S_8-$CoSe_2$	GC	5	150	89	[2]
$NiSe_2$@NC-PZ [c]	GC	5	162	88	[3]
c-$CoSe_2$	CC [b]	5	190	85	[4]
$CoSe_2$–$MoSe_2$/G	GC	5	198	79	[5]
Ni-$MoSe_2$	GC	5	206	81	[6]
11%Ni-WSe_2	GC	10	215	109	[7]
0.4%Pd_1-$CoSe_2$	GC RDE [d]	10	240	92	[8]
Co-WSe_2/MWCNT	GC	5	241	-	[9]

[a] all the values are presented in RHE; [b] CC – carbon cloth; [c] NC-PZ – N-doped carbon-pyrazine; [d] RDE – rotating disk electrode.

Supplementary note - Electrochemical measurements

- For the HER, rate-determining steps (RDS) mechanisms have been thoroughly studied, for which there are two widely accepted mechanisms. Both are two-step mechanisms that begin with the adsorption of a proton onto the electrode surface through an electrochemical reduction process (Volmer step).
  Volmer adsorption step:

$$H_3O^+ + e^- \rightarrow H^\bullet_{ads} + H_2O \qquad b \approx 120mV/dec \quad (1)$$

This step is followed either by the recombination of two hydrogen atoms adsorbed on the surface (Tafel desorption step):

$$H^\bullet_{ads} + H^\bullet_{ads} \rightarrow \uparrow H_2 \qquad b \approx 30mV/dec \quad (2)$$

or by the direct bonding of a hydrated proton with the adsorbed hydrogen atom which includes an electron transfer from the electrode surface (Heyrovsky step).

$$H_{ads} + H_3O^+ + e^- \rightarrow \uparrow H_2 + H_2O \quad b \approx 40mV/dec \quad (3)$$

The HER mechanism begins with the adsorption of H at the electrocatalyst surface, which is referred to as the Volmer step. Our experimental values point to the next step being the reaction of an adsorbed H with an H^+ from the electrolyte (*i.e.*, the Heyrovsky step) to form H_2, this being the RDS mechanism.

The adsorption free energy of H on Pt is close to the thermoneutral state ($\Delta G_{H^*} \approx 0$), thus considered as the best HER electrocatalyst [10]. At the measured thickness, $PtSe_2$ is multilayer, in which the density of states (DOS) at the Fermi level is predicted to be very low due to its semimetallic character [11]. Although $PtSe_2$ supposedly has excellent HER activity according to the ΔG calculation [12], there are additional factors such as the interlayer conductivity that may influence its performance.

On the other hand, theoretical findings suggest that graphene is ideal for contacting $PtSe_2$ in electronic applications [13]. It has also been predicted by DOS calculations that the addition of rGO causes decreases in bandgaps of both pristine and composite TMDs, changing the accumulation in the conduction band and valence bands, suggesting higher electron mobility [14].

Overall, there is a trend that the HER activities of the semimetallic are higher than their respective semiconducting counterparts [15,16]. However, stability and activity are highly dependent on both the transition metal and the chalcogen, but it is difficult to establish direct correlations.

- From the comparison of the electrochemically active surface areas (ECSA), the double layer capacitances (C_{dl}), CV measurements were done in a non-faradaic region, in 1.0 M KOH at various scan rates, ranging from 20-200 mV s^{-1} and 0.9 <*E*<1.3 V *vs*. RHE. The C_{dl} were determined according to the equation [17]:

$$C_{dl} = \frac{(j_a + |j_c|)}{2v} = \frac{\Delta j}{2v}$$

in which j_a and j_c are the anodic and cathodic current density, respectively, recorded at *E*=1.1 V *vs*. RHE, and v is the scan rate.

- Nyquist plots were obtained for the catalysts at -80 mV *vs.* RHE in 1.0 M KOH. Equivalent circuits were used to fit the experimental data. For all cases, R_s represents the solution resistance. For 10% Pt/C@GC, and C_{paper}, CPE is the constant phase element and R_{ct} is the charge transfer resistance. For the $PtSe_2$/rGO foil, (CPE_1-R_1) is due to the semicircle appearing at a high-frequency zone due to the

substrate. (CPE_2-R_{ct}) is due to the charge transfer process of the catalytic material for HER. It has been described as the first small semi-circle and the second larger semi-circle, respectively [18].

- Turnover frequency (TOF) calculations of the $PtSe_2$/rGO foil were done following the proposed formulas [19,20]

$$TOF\ (H_2/s) = \frac{n\ H_2\ tunrovers/cm^2}{n\ active\ site\ /\ cm^2}$$

The number of total hydrogen turnover was calculated from *I* in the LSVs

$$n\ H_2 \frac{tunrovers}{cm^2} = \left(\frac{mA}{cm^2}\right).\left(\frac{1\ mol\ e^-}{96485.3\ C}\right).\left(\frac{1\ mol}{2\ mol\ e^-}\right).\left(\frac{6.022x10^{23}\ molecules\ H_2}{mol\ H_2}\right)$$
$$= 3.12x10^{15}\ \frac{H_2/s}{cm^2}\ per\ \frac{mA}{cm^2}$$

The of actives sites in the $PtSe_2$/rGO foil were calculated from the content of Pt determined by ICP, considering each Pt atom account as an active site

$$Pt\ sites/cm^2 = \left(\frac{Pt\ loading\ \left(\frac{g}{cm^2}\right)}{Pt\ Mw\ \left(\frac{g}{mol}\right)}\right).\left(\frac{6.022x10^{23}\ molecules\ H_2}{mol\ H_2}\right)$$

References

1 C. Liu, Y. Hu, F. Liu, H. Liu, X. Xu, Y. Xue, J. Zhang, Y. Li and C. Tang, *Int. J. Hydrogen Energy*, 2021, **46**, 17133–17142.

2 S. Chakrabartty, S. Karmakar and C. R. Raj, *ACS Appl. Nano Mater.*, 2020, **3**, 11326–11334.

3 Z. Huang, S. Yuan, T. Zhang, B. Cai, B. Xu, X. Lu, L. Fan, F. Dai and D. Sun, *Appl. Catal. B Environ.*, 2020, **272**, 118976.

4 P. Chen, K. Xu, S. Tao, T. Zhou, Y. Tong, H. Ding, L. Zhang, W. Chu, C. Wu and Y. Xie, *Adv. Mater.*, 2016, **28**, 7527–7532.

5 X. Wang, B. Zheng, B. Wang, H. Wang, B. Sun, J. He, W. Zhang and Y. Chen, *Electrochim. Acta*, 2019, **299**, 197–205.

6 G. Zhao, X. Wang, S. Wang, K. Rui, Y. Chen, H. Yu, J. Ma, S. X. Dou and W. Sun, *Chem. – An Asian J.*, 2019, **14**, 301–306.

7 S. R. Kadam, A. N. Enyashin, L. Houben, R. Bar-Ziv and M. Bar-Sadan, *J. Mater. Chem. A*, 2020, **8**, 1403–1416.

8 X. Zhao, X. Li, D. Xiao, M. Gong, L. An, P. Gao, J. Yang and D. Wang, *Appl. Catal. B Environ.*, 2021, **295**, 120280.

9 G. Zhang, X. Zheng, Q. Xu, J. Zhang, W. Liu and J. Chen, *J. Mater. Chem. A*, 2018, **6**, 4793–4800.

10 N. Dubouis and A. Grimaud, *Chem. Sci.*, 2019, **10**, 9165–9181.

11 G. Y. Guo and W. Y. Liang, *J. Phys. C Solid State Phys*, 1986, **19**, 995–1008.

12 X. Chia, A. Adriano, P. Lazar, Z. Sofer, J. Luxa and M. Pumera, *Adv. Funct. Mater.*, 2016, **26**, 4306–4318.
13 S. Sattar and U. Schwingenschlögl, *ACS Appl. Mater. Interfaces*, 2017, **9**, 15809–15813.
14 Y. Lei, S. Pakhira, K. Fujisawa, X. Wang, O. O. Iyiola, N. Perea López, A. Laura Elías, L. Pulickal Rajukumar, C. Zhou, B. Kabius, N. Alem, M. Endo, R. Lv, J. L. Mendoza-Cortes and M. Terrones, *ACS Nano*, 2017, **11**, 5103–5112.
15 Y. Gong, Z. Lin, Y. X. Chen, Q. Khan, C. Wang, B. Zhang, G. Nie, N. Xie and D. Li, *Nano-Micro Lett.*, 2020, **12**, 1–34.
16 B. Cao, Z. Ye, L. Yang, L. Gou and Z. Wang, *Nanotechnology*, 2021, **32**, 412001.
17 E. Gileadi, *Electrode Kinetics for Chemists, Chemical Engineers and Materials Scientists*, Wiley-VCH, 1993.
18 S. Anantharaj and S. Noda, *ChemElectroChem*, 2020, **7**, 2297–2308.
19 P. Kuang, Y. Wang, B. Zhu, F. Xia, C. W. Tung, J. Wu, H. M. Chen and J. Yu, *Adv. Mater.*, 2021, **33**, 2008599.
20 H. Fei, J. Dong, M. J. Arellano-Jiménez, G. Ye, N. Dong Kim, E. L. G. Samuel, Z. Peng, Z. Zhu, F. Qin, J. Bao, M. J. Yacaman, P. M. Ajayan, D. Chen and J. M. Tour, *Nat. Commun.*, 2015, **6**, 1–8.